Efficient Simulation of Incompressible Viscous Flow over Single and Multielement Airfoils

Stuart E. Rogers,* N. Lyn Wiltberger,† and Dochan Kwak‡
NASA Ames Research Center, Moffett Field, California 94035

The incompressible, viscous, turbulent flow over single and multielement airfoils is numerically simulated in an efficient manner by solving the incompressible Navier-Stokes equations. The solution algorithm uses the method of pseudocompressibility with an upwind-differencing scheme for the convective fluxes, and an implicit line-relaxation scheme. The motivation for this work includes interest in studying high-lift takeoff and landing configurations of various aircraft. In particular, accurate computation of lift and drag at various angles of attack up to stall is desired. Two different turbulence models are tested in computing the flow over a NACA 4412 airfoil; an accurate prediction of stall is obtained. The approach used for multielement airfoils involves the use of multiple zones of structured grids fitted to each element. Two different approaches are compared: 1) a patched system of grids, and 2) an overlaid Chimera system of grids. Computational results are presented for two-element, three-element, and four-element airfoil configurations. Generally, good agreement with experimental surface pressure coefficients is seen. The code converges in less than 200 iterations, requiring on the order of 1 min of CPU time on a CRAY YMP per element in the airfoil configuration.

Introduction

AN increased understanding of high-lift systems will play an important role in designing the next generation of transport aircraft. Current designs for such aircraft typically involve multiple elements, such as leading-edge slats and multiple-slotted flaps. The current trend is toward a more efficient, yet simpler design which will lead to reduced manufacturing and maintenance costs. At the same time, increases in lift coefficients for a given angle of attack and increases in maximum lift coefficient will lead to a larger payload capability. Improved designs will also allow for reduced noise in areas surrounding airports. Understanding of high-lift flow physics harbors the potential to improve airport capacity through a reduction of an airplane's wake vortices, allowing closer spacing between subsequent airplanes taking off and landing.

Increased knowledge of the flow physics involved with high-lift systems is therefore of greater interest than ever before as the need to improve over current designs becomes acute. Study of these configurations will require both computational and experimental efforts. Computational fluid dynamics (CFD) is playing a large role in this work. Multielement configurations present a number of challenging problems to the numerical investigators. These include problems involving turbulent boundary-layer separation, confluent boundary layers and wakes, Reynolds number effects, three-dimensional effects, compressibility effects, transition, and complex geometries. Although the problems are inherently three-dimensional, there is still much to be learned about the flow physics by studying two-dimensional models.

The computational tools available range from the more efficient inviscid/viscous coupled methods, to a Reynolds-averaged Navier-Stokes (RANS) analysis. An example of the former method is given by Kusunose et al.[1] They use a full potential method coupled with an integral boundary-layer method. These methods have been found to be successful in accurately computing the pressure distribution for multielement airfoils, including cases up to maximum lift, some of which involve separation. The coupled method has been proven to be useful as an effective engineering design tool. This method is limited by its inability to compute beyond maximum lift conditions, and may have problems with certain features of some airfoil systems such as flap wells, thick trailing edges, or unsteady effects.

Navier-Stokes calculations for high-lift systems have been investigated by a number of authors.[2-4] Schuster and Birckelbaw[2] computed the flow over a two-element airfoil using a structured, compressible, RANS solver. The grid system used was a pointwise patched system with three zones, with C-grids around both the main element and flap, and another outer C-grid surrounding those. Good results were obtained for low-Reynolds number turbulent flow. The next two authors, Barth[3] and Mavriplis,[4] both used an unstructured grid approach to handle the difficulty of discretizing multelement geometries. They were each able to produce accurate pressure coefficient information on the airfoil surfaces. The accuracy of the unstructured grid approach, however, is limited because of the very large aspect ratio of the triangular cells required to resolve high-Reynolds number boundary-layer flows. Also, this approach is not well-developed for three-dimensional problems. Large computational resources are required, especially CPU memory, to make these methods work for viscous flows. Unstructured methods are currently generating a lot of interest in the research community; improvements to these limitations are to be expected in the near future. Until such a time, the current authors believe that a structured grid approach is the most suitable for solving viscous multielement problems in two and three dimensions.

The current work uses an incompressible RANS flow solver to compute the flow over multielement airfoils. Two different grid approaches are used; the first approach employs the patched grids utilized in Ref. 2, and the second uses an overlaid grid approach known as the Chimera scheme.[5] The current work examines several airfoil flow problems in two dimensions in an effort to characterize current capability to numerically study

such problems. Grid topology, computational efficiency, turbulence modeling, and resulting accuracy are issues to be examined in the current work.

An incompressible flow solver is being utilized because the flow conditions for takeoff and landing will generally have a Mach number of 0.2 or less. Recent experimental results by Valarezo et al.[6] show the effect of Mach number on flow over several multielement configurations. These results show very little difference in the lift coefficient vs angle-of-attack curves between Mach numbers of 0.15–0.20 for most configurations. For a Mach number of 0.26, the compressible effects become significant, as there is a significant drop in maximum lift and stall angle compared with the lower Mach numbers. There will be conditions where a freestream Mach number of 0.2 will cause a small localized region of sonic flow at a slat leading edge, which could lead to dramatic compressible effects, such as the formation of a shock. If this interacts with the boundary layer, it will cause separation and lead to a dramatic loss of lift. This does not occur in the experimental results of any of the cases studied in this work, and we have found the incompressible approach to be valid for a large range of high-lift conditions; this approach will certainly provide an adequate tool for studying the issues outlined above. When a case is encountered where compressible effects are important, the lessons learned here about grid generation, grid topology, and turbulence modeling will be valuable when applying a compressible Navier-Stokes solver.

The advantage to using an incompressible solver is that it requires significantly less computing time. Experience has shown that a multielement calculation using a chimera grid scheme can be solved 5–10 times faster using the current incompressible Navier-Stokes, compared to a compressible Navier-Stokes solver. This is both because the incompressible formulation results in one less equation, and because compressible flow solvers can be very slow to converge at these low freestream Mach numbers.

Algorithm

The current computations are performed using the INS2D computer code which solves the incompressible Navier-Stokes equations for steady-state flows[7] and unsteady computations.[8] This algorithm has also been applied to problems in three dimensions using the INS3D-UP code.[9] The code is based on the method of artificial compressibility as developed by Chorin[10] in which a pseudotime derivative of pressure is added to the continuity equation. Thus, the convective part of the equations form a hyperbolic system, which can be iterated in pseudotime until a steady-state solution is found. For unsteady problems, subiterations in pseudotime are performed for each physical time step. Since the convective terms of the resulting equations are hyperbolic, upwind differencing can be applied to these terms. The current code uses flux-differencing splitting modeled after the scheme of Roe.[11] The upwind differencing leads to a more diagonally dominant system than does central differencing, and does not require the additional use of artifical dissipation. The system of equations is solved using a Gauss-Seidel type line-relaxation scheme. The line-relaxation scheme is very useful for computing multizonal grids because it makes it possible to iteratively pass ΔQ (which is the change in the dependent variables for one time step) information between the zonal boundaries as the line-relaxation sweeping takes place. The result is a semi-implicit passing of boundary conditions between zones, which further enhances the code stability.[12] The resulting code is very robust and stable. It is capable of producing steady-state solutions to fine-mesh problems in 100 to 200 iterations. More detail about the computer code can be found in Refs. 6–8.

Most of the present calculations used the turbulence model developed by Baldwin and Barth,[13,14] where the specific formulation found in Ref. 13 was used. This is a one-equation turbulence model that avoids the need for an algebraic length scale and is derived from a simplified form of the standard

k-ε model equations. In the current application, the equation is solved using a line-relaxation procedure similar to that used for the mean-flow equations. This model has been found to be very robust and easy to implement for multiple-body configurations. The next section includes computations of flow over a single airfoil. One of the studies for this problem includes a comparison of the Baldwin-Barth turbulence model with the Baldwin-Lomax[15] algebraic turbulence model.

Computed Results

NACA 4412 Airfoil

Calculations were performed for the flow over a NACA 4412 airfoil at a Reynolds number of 1.52 million. A C-grid with dimensions of 241 × 63 was used, with wall spacings on the order of 10^{-5}, which corresponds to y^+ values on the order of one. The grid was computed using a hyperbolic grid generator.[16] A close view of this grid is shown in Fig. 1. In order to compute flow quantities for the points on the computational boundary in the "wake cut" line of the c-mesh, two lines of dummy points are added such that these dummy points coincide with points on the other side of the wake line. The first line of these dummy points is updated by injecting values from the coincident interior points on which they lie. Using this overlap produces smooth solutions to the equations across this computational boundary. This procedure also adds dummy points inside the airfoil. These points are merely blanked out and never used in the solution procedure. All of the C-grids in this work use this overlap.

This flow was computed using two different turbulence models: 1) the Baldwin-Barth model[13] and 2) the Baldwin-Lomax model.[15] Figure 2 shows a comparison between these computations and the experimental results of Coles and Wadcock[17] at an angle of attack of 13.87 deg, which is very nearly maximum lift conditions. In the experiment the flow separated at approximately 85% of chord. Trip-strips were employed in the experiment on the suction and pressure sur-
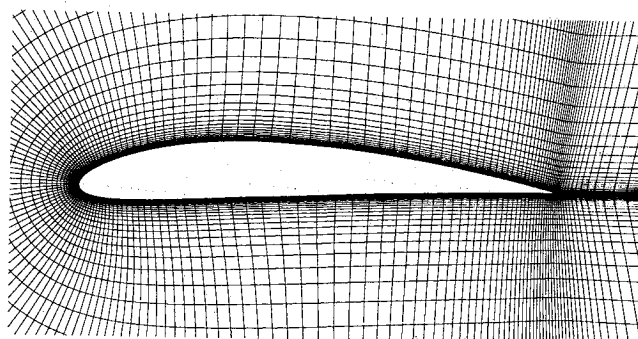

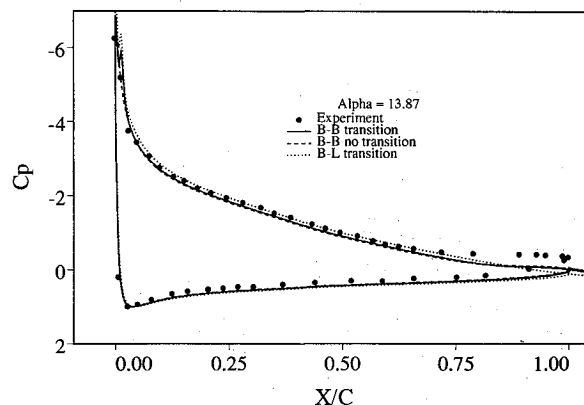Fig. 1 241 × 63 grid used for flow over a NACA 4412 airfoil.

Fig. 2 Pressure coefficient on surface of a NACA 4412 airfoil at Reynolds number of 1.52 million.

faces at chord locations of x/c of 0.023 and 0.1, respectively. The computations thus specify these as the transition points. For the Baldwin-Barth model this is implemented by setting the production terms to zero upstream of these locations; for the Baldwin-Lomax model the eddy viscosity is set to zero upstream of the transition location. The agreement is fairly good, with the biggest discrepancy occurring at the trailing edge where the predicted pressure is too high. However, the Baldwin-Barth model does give a flattening of the pressure over the aft 15% of chord, indicating flow separation, where the Baldwin-Lomax solution does not show this tendency. This figure also shows that the computations with the transition predict a leading-edge laminar separation bubble. The experiment reports that there was no laminar separation bubble at this angle of attack, so an additional computation was run using the Baldwin-Barth model with the production terms turned on everywhere, thus the boundary layer was fully turbulent. The pressure coefficient for this is also shown in Fig. 2. There is a slight improvement in the trailing-edge area for this solution. The Baldwin-Lomax model showed no difference in the pressure or velocity solution when it was run without specifying transition, except that it removed the laminar separation bubble.

Velocity profiles from the suction surface boundary layer are plotted in Fig. 3 at streamwise stations of x/c = 0.62, 0.675, 0.731, 0.786, 0.842, 0.897, and 0.953. The profiles are shown using the streamwise component of velocity in boundary-layer coordinates, i.e., the velocity component tangential to the local airfoil surface. This figure shows in greater detail the problems of the Baldwin-Lomax solutions in this region: the boundary-layer profile is too full, and the solution shows only a tiny region of separation. The Baldwin-Barth solution is in closer agreement with the experimental results, but also suffers from too small of a separation region. The case without transition shows the best agreement with the experimental profiles.

One factor which could help explain the difference between the experimental and computational results is the lack of wind-tunnel wall effects in the computations. This is supported by the fact that the pressure side of the airfoil does not agree, and by the evidence in the velocity profile plots which indicate that the edge velocities are in disagreement. Unfortunately, the experimental reference[17] does not give a description of the test-section geometry, making it difficult to compute these effects.

Computations were run for a range of angles of attack from zero lift to maximum lift. The lift coefficient vs angle of attack is plotted in Fig. 4. This shows that the Baldwin-Barth solution with transition gives very good agreement in the lift, including the prediction of stall. For all cases, as the angle of maximum lift was approached, the flow tended toward unsteadiness. That is, the steady-state computations did not converge completely, which, for the artificial compressibility formulation means that the results do not satisfy the continuity equation.
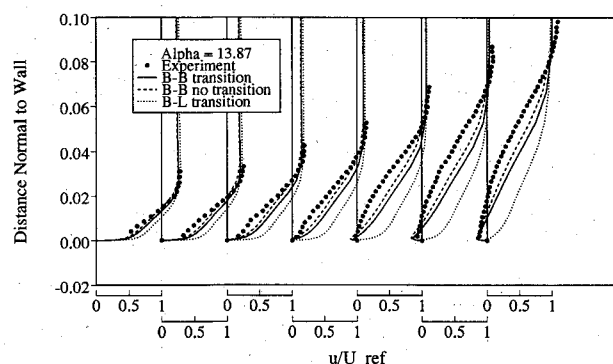

Fig. 3   Velocity profiles on upper surface of a NACA 4412 airfoil at streamwise stations of x/c = 0.62, 0.675, 0.731, 0.786, 0.842, 0.897, and 0.953.
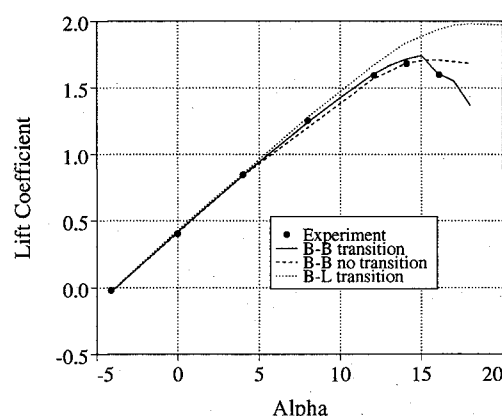

Fig. 4   Lift coefficient vs angle of attack for flow over a NACA 4412 airfoil.
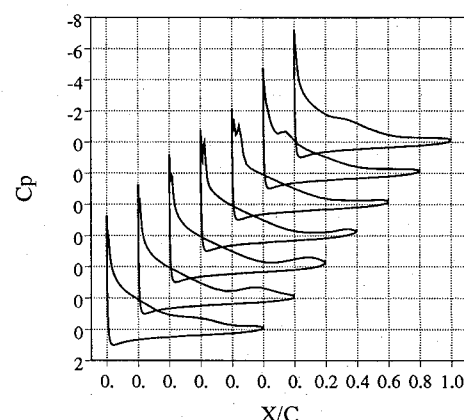

Fig. 5   Pressure coefficient on the surface of the NACA airfoil at 16-deg angle of attack for seven different times during the unsteady periodic motion.

In these cases the code was then run in a time-accurate, unsteady mode. For the Baldwin-Barth model with transition, at an angle of attack of 14 deg, the unsteadiness dies out when the computations are run in a time-accurate mode. At 16 deg, an unsteady periodic behavior ensues; as shown in the figure, the mean lift drops sharply below the values from smaller angles of attack. Examination of the flow shows that the leading-edge laminar separation bubble is periodically shedding and traveling through the boundary layer on the top surface of the airfoil and past the trailing edge. Figure 5 shows the pressure coefficient on the surface of the airfoil at seven different times through the period of this flow. The forming of the leading-edge vortex is evident, and it can be seen that it travels downstream and past the trailing edge.

For the Baldwin-Barth model without transition at an angle of attack of 16 deg, all oscillations damp out and it converges to a steady-state solution. At 18 deg, the lift continues to oscillate periodically, yet there is only a slight drop in the lift, and there is a complete absence of a leading-edge separation bubble. The Baldwin-Lomax computations do not have any type of periodic unsteady behavior with or without transition. The results from this model show that a drop in lift does not occur until an angle of attack of 20 deg.

In short, the Baldwin-Barth model shows promise for use in predicting high-lift flows, and although some deficiencies are shown here, it is significantly better than the Baldwin-Lomax model. In addition, the Baldwin-Barth model is much easier to use than the Baldwin-Lomax model, in that it does not require a length scale; it is straightforward to implement for a multielement airfoil computation. All of the results in the later sections of this article use the Baldwin-Barth model.

The convergence history is shown in Fig. 6 for the angle of attack of 13.87 deg for both turbulence models with and with-
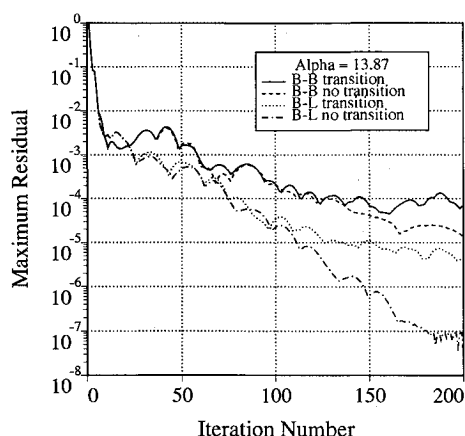
Fig. 6 Convergence history showing maximum residual vs iteration number for flow over a NACA 4412 airfoil at 13.87-deg angle of attack.

out transition. In general, fast convergence is seen, with converged solutions obtained in 100–200 iterations. Specifying the transition tends to produce an unsteady component into the flowfield which somewhat delays the convergence. It can also be seen that the Baldwin-Lomax computations converge much faster than the Baldwin-Barth model. The computing time on a Cray YMP required for this 241×63 mesh is 100 s for 200 iterations when using the Baldwin-Barth model, and 90 s for 200 iterations when using the Baldwin-Lomax model. When running the unsteady cases, the algorithm requires subiterations at each physical time step to drive the divergence of velocity toward zero. When running the unsteady 16-deg angle-of-attack case with a nondimensional time step of 0.05, 40 physical time steps resulted in one period of the flow. This took about 10 min of computing time. Due to the difficult nature of solving the unsteady incompressible Navier-Stokes equations, it probably would not be computationally cheaper to use an incompressible formulation over a compressible Navier-Stokes code to study poststall, unsteady airfoil flows.

Two-Element Airfoil

The geometry is made up of a NACA 4412 airfoil with a NACA 4415 flap deployed at 21.8 deg, with the entire configuration at 8.2 deg angle of attack. This geometry was studied experimentally by Adair and Horne.[18] The chord Reynolds number was 1.8 million, and the Mach number in the experiment was 0.09. The blockage in the wind tunnel was severe enough that the wind-tunnel walls needed to be included in the calculations in order to get good agreement with the experimental pressure coefficients.

The airfoils were discretized using two different grid approaches. The first follows the work of Schuster and Birckelbaw[2] and uses three zones which are patched together using coincident points. This grid is shown in Fig. 7. Each of the elements is surrounded by a C-grid, and these two grids are surrounded by another C-grid which extends out to the wind-tunnel walls. The dimension of these grids are 374×44, 241×33, and 352×32, respectively, for a total of 35,000 points.

The second type of grid uses a Chimera[5] approach, in which C-grids were generated about each of the elements. To include the effects of the wind-tunnel walls, these grids were inset into a third zone composed of an h-grid. A partial view of these three grids is shown at the top of Fig. 8, with a closeup of the main-element grid in the vicinity of the flap shown in the bottom half of this figure. These grids had dimensions of 261×49, 203×35, and 121×61, for a total of 27,500 points. To implement the Chimera approach, these grids are given to the PEGSUS[4] code. This code first punches holes into grids where they overlap a body (as shown in the bottom of Fig. 8). It then computes the interpolation stencils used to update the flow quantities at the fringe points of these holes, and to update the flow quantities at the outer boundaries of
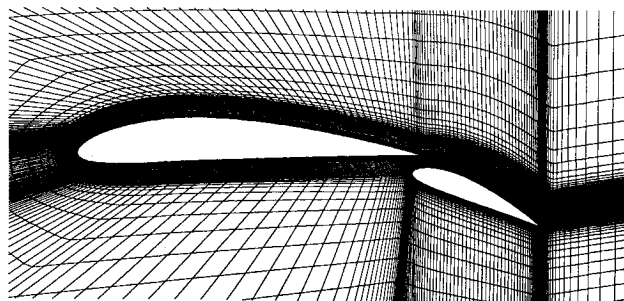

Fig. 7 Three-zone patched grid used to compute flow over a NACA 4412 airfoil with a NACA 4415 flap.
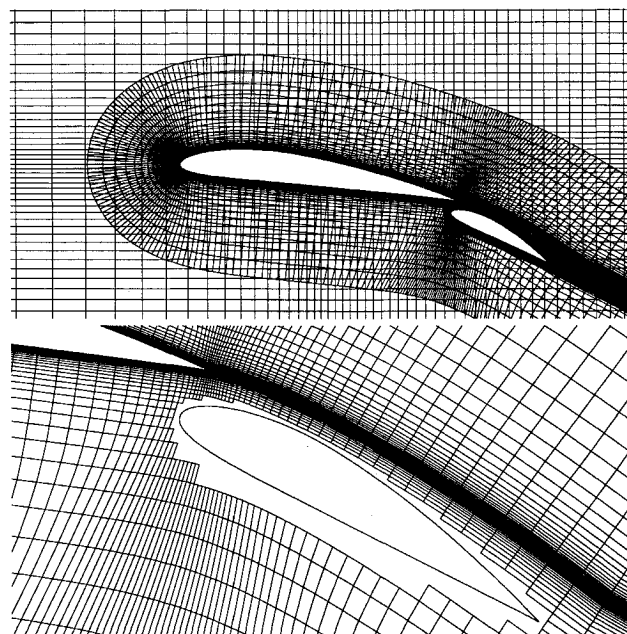

Fig. 8 Overlaid Chimera grid used to compute flow over a NACA 4412 airfoil with a NACA 4415 flap.
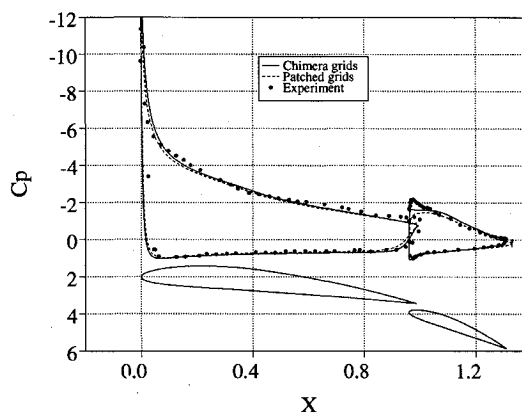

Fig. 9 Pressure coefficient on surface of two-element airfoil comparing both patched grid and overlaid grid schemes to experimental results.

grids which lie inside another grid (like the outer boundaries of the C-grids seen in the top of Fig. 8). For both the Chimera and the patched grid approaches, the spacing next to the surfaces was set to 2×10^{-5}, which correspond to y^+ values at the wall on the order of one.

The computational results compare well with the experimental results of Adair and Horne.[18] A plot of the pressure coefficient on the surface of the elements is shown in Fig. 9. Results from both of the grid approaches is shown. The biggest difference between the computation and experiment is

seen in the suction peak at the leading edge of the flap. The difference might be explained by a difference in the geometry between the computations and the experiment. There was an ambiguity in the way in which the flap position is defined.

Figure 10 shows the convergence history for these computations. They both converge very well, giving a steady-state solution in about 100 iterations. Each of these grid cases takes about 100 s of CPU time on a Cray YMP for 100 iterations. The code runs at about a rate of 80 MFLOPS, and requires 36×10^{-6} CPU s/grid point/iteration. Since the Chimera approach uses about 20% fewer grid points, it takes a little less computing time. The major difference between these approaches is the amount of time and effort it takes to generate the grids. The patched grid case takes on the order of several hours of work; it involves generating inner boundaries which define the surface with the proper point distribution to ensure that the grids can be patched together. Then hyperbolic grids are matched halfway across the gap from each of the elements. The resulting outer boundaries of these are merged into a common interface where they match. The inner grids are recalculated to match this interface. Finally, the outer C-grid is marched outward using a hyperbolic grid generator. The process is tedious and is not easily repeatable for a different case (new flap placement, or flap angle), or for a different geometry. On the other hand, the overlaid grids can be generated in only a matter of minutes; one need only generate two independent hyperbolic grids about each of the elements, and then feed these into the PEGSUS code[5] as described above. Once this has been set up for one case, it is very easy to reproduce it for another case or another geometry. It is for these reasons that the overlaid grid approach was adopted for the rest of the cases and geometries in this work.

Figure 11 shows velocity profiles from the Chimera calculations at three locations on the top surface of the main element and flap. These are plotted with experimental measurements of the profiles by Adair and Horne.[18] These plots show fairly good agreement with the experimental results. The biggest discrepancy is the difference in the gap velocity off the surface of the flap's leading edge. This is related to the difference seen in the pressure coefficient plot in Fig. 9. The velocity profile from the trailing edge of the flap shows that there is a separation occurring over the top surface of the flap. This profile shows that the computational separation bubble is not as thick as that seen in the experiment, but that the computations do an excellent job of capturing the wake from the main element in this region.

Further calculations were carried out using freestream outer boundaries (neglecting wind-tunnel walls). These calculations
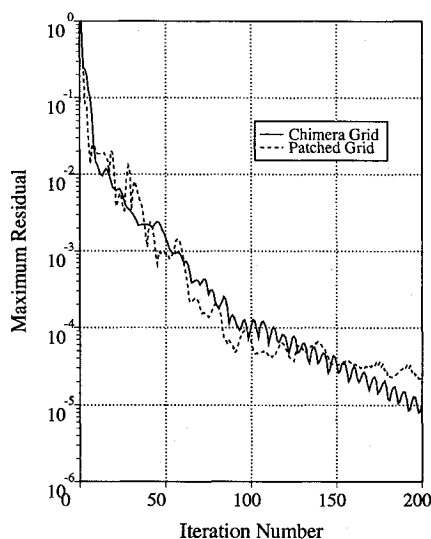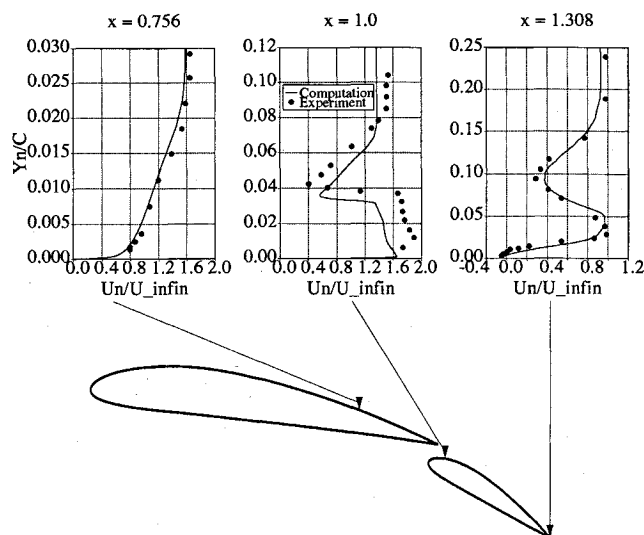

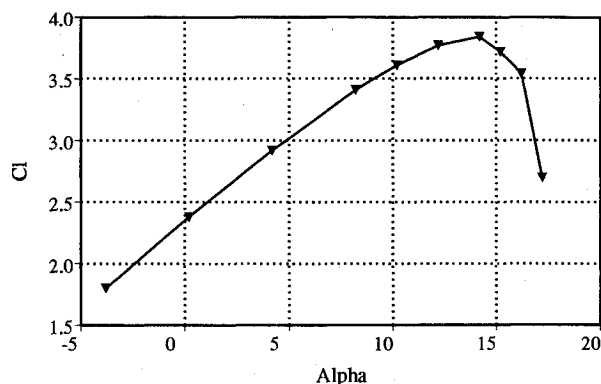Fig. 11   Velocity profiles from overlaid grid calculations compared to experimental data.

Fig. 12   Coefficient of lift vs angle of attack as computed by the overlaid grid approach for the two-element airfoil.

use the overlaid grids with two zones, where the main element grid extends beyond 10 chord lengths from the airfoil. These were run at various angles of attack to show the capability to compute maximum lift conditions as well as poststall conditions. The curve of lift coefficient vs angle of attack is shown in Fig. 12. The lift drops off sharply at $\alpha = 15$ deg, and the calculations indicate that the flow becomes unsteady beyond that angle of attack. The skin friction along the surfaces of the airfoil elements is shown in Fig. 13. It can be seen that the flow separates at the trailing edge of the flap even at zero angle of attack, and that this separation reduces in size with increasing angle of attack. The main element has trailing-edge separation occurring at angles of attack of 12 deg and greater. It becomes massively separated at an angle of attack of 16 deg. At this angle of attack the flap shows evidence of a vortex passing over the top because of the large dip in the skin friction on the surface of the flap.

Three-Element Airfoil

The three-element computational configuration was taken from an experimental geometry of a supercritical airfoil which has been tested by Valarezo et al.[19] This airfoil consisted of a leading-edge slat deployed at -30 deg, a main element, and a trailing-edge flap deployed at 30 deg. The experimental Mach number was 0.2 and the chord Reynolds number was 9 million. The Chimera approach was used to discretize the geometry and produce a computational grid. A C-grid was placed around each element, with the main-element grid extending out to the far field. The grids for the slat-, main-, and flap-element had dimensions of 221×41, 401×75, and 221×47, respectively, for a total just under 51,000 points. The

Fig. 10   Convergence history for flow over two-element airfoil for patched grid and overlaid grid schemes.
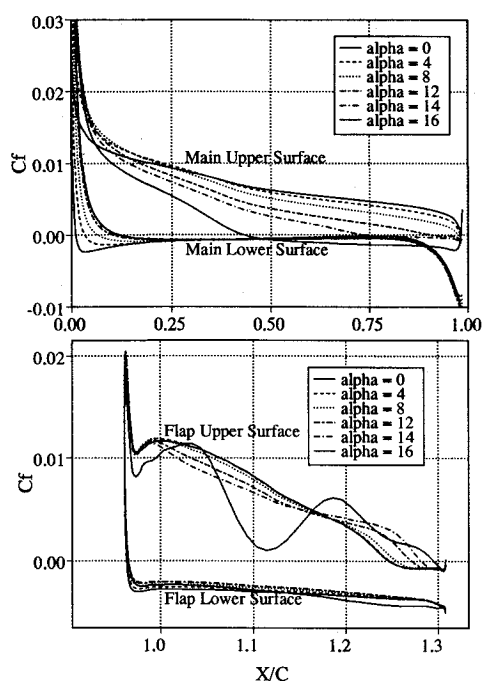
Fig. 13 Skin friction on the surface of the main element and flap for various angles of attack.
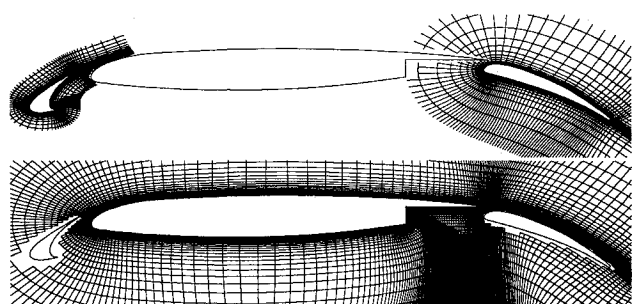

Fig. 14 Grid and geometry for the three-element airfoil, showing every other grid point around the slat and flap.
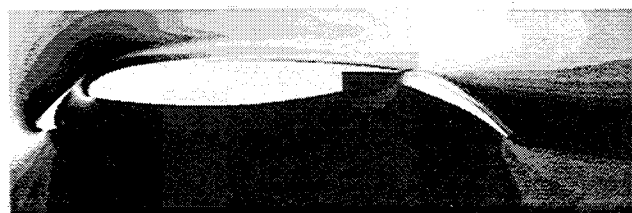

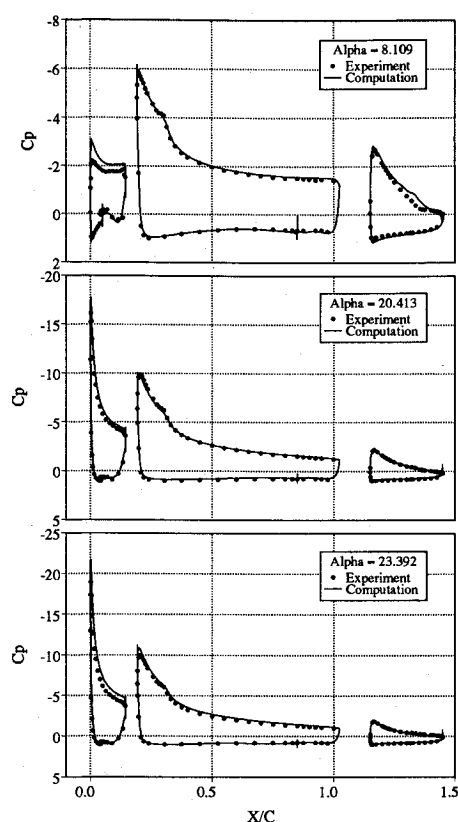Fig. 15 Velocity magnitude contours at 20.4-deg angle of attack.

Fig. 16 Pressure coefficient comparing computation and experiment for angles of attack of 8.1, 20.4, and 23.4 deg.

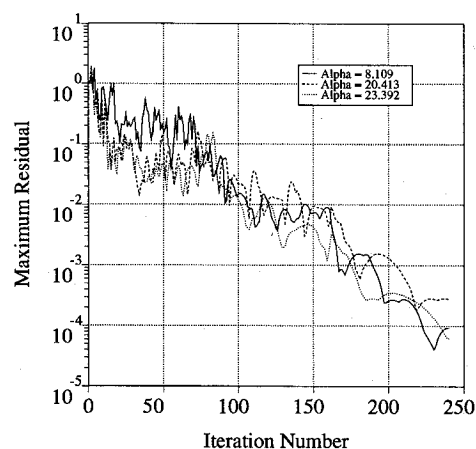Fig. 17 Convergence history for three-element airfoil.

top of Fig. 14 shows every other grid point in the first and third element grids, with the resulting holes caused by the main element. The second half of this figure shows the main element grid. The wake cut boundary of this grid has been aligned just above the top surface of the flap element in an attempt to put as many points as possible in the wake and boundary-layer region found there.

Figure 15 shows velocity magnitude contours of the three-element configuration run at 20.4-deg angle of attack. The wake of the slat is clearly seen across the top of the succeeding elements. The experimental results of Valarezo et al.,[19] and the computational results of this study are compared in Fig. 16. These figures show pressure coefficients on the surfaces of each element at three different angles of attack, 8.1, 20.4, and 23.4 deg. Very good agreement is seen except on the suction side of the slat. Also, there is a discrepancy on the

upper surface of the flap trailing edge. The experimental results show a strong adverse pressure gradient followed by a flattening in the pressure coefficient curve, which is generally evidence of flow separation. The computational results do not show this. This is probably due to the general trend of the turbulence model to underpredict the amount of separation. The experiment allowed free transition on the elements, and the computations assumed a turbulent boundary layer everywhere. Further work in this area could include use of a transition model for this calculation.

Convergence histories of these computations are shown in Fig. 17. These computations converge well, with steady-state solutions being obtained after 200 iterations, which corresponds to about 4 min of CPU time on a Cray YMP.

Four-Element Airfoil

The geometry is made up of a NASA 9.3% blunt-based, supercritical airfoil with a leading-edge slat deployed at −47.2

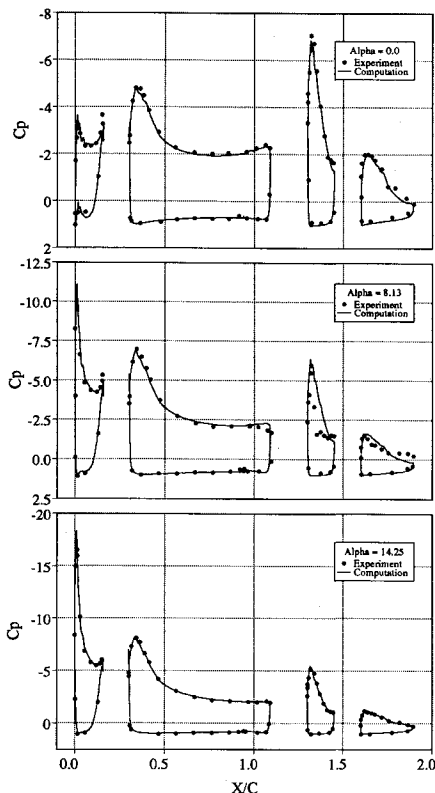Fig. 18   Velocity magnitude contours at 14.25-deg angle of attack.

Fig. 19   Pressure coefficient comparing computation and experiment for angles of attack of 0.0, 8.1, and 14.25 deg.
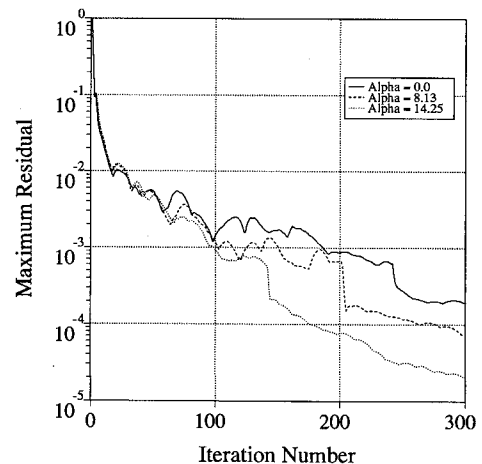

Fig. 20   Convergence history for four-element airfoil.

the flow over the flap underpredicts the amount of separation at the lower angles of attack.

The convergence histories for the four-element configuration at three different angles of attack are shown in Fig. 20. The computations converge well and a steady-state solution is produced after about 200 iterations, which corresponds to approximately 4 min of CPU time on the Cray YMP.

Conclusions

An incompressible flow solver has been used to compute flow over several airfoil geometries for the purpose of developing a tool to study takeoff and landing configurations. The code is robust and produces numerical simulations in a matter of minutes. The flow over a NACA 4412 airfoil was investigated, and the Baldwin-Barth and Baldwin-Lomax turbulence models were compared. The Baldwin-Barth model gave significantly better results, and was much eaiser to use, particularly for multielement flows. The use of the Chimera overlaid grid approach was found to be much easier than using a patched grid scheme for solving multiple element airfoil flows. Both approaches are capable of producing fairly accurate solutions. The computed pressure prediction was shown for geometries with two, three, and four airfoil elements. The common discrepancy between these calculations and experimental results involves separated flow. The results for the NACA 4412 airfoil indicate that deficiencies with the turbulence model and lack of inclusion of the wind-tunnel wall effects are the most likely causes of these inaccuracies. Work in progress with different turbulence models shows promise in remedying this. Investigation of other turbulence models and their implementation for a multielement airfoil calculation will be the focus of future work. In addition, future work will include the extension of the current work to three dimensions.

deg, and two trailing-edge flaps at 30 and 49.7 deg, respectively. This configuration matches the geometry used in the experimental work done by Omar et al.[20] The Mach number in the experiment was 0.201 and the chord Reynolds number was 2.83 million. The geometry was discretized using the Chimera approach. C-grids were generated around each of the elements, with the main element grid being marched out to the outer boundary. These grids were overlaid and the PEGSUS[5] code was used to create an overlaid grid. Approximately 55,000 points were used in the resulting composite grid in order to resolve the flow physics adequately in the boundary layers and wakes. The grid spacing next to the surfaces of the airfoils was 10^{-5} which ensures y^+ values of 1 near the wall.

The computational results of this study were compared with the experimental results of Omar et al.[20] Figure 18 shows velocity magnitude contours around the four-element configuration at 14.25-deg angle of attack. In this figure the wake from the leading-edge slat is apparent over the main element. Subsequent wakes from the main element and flaps can also be observed. Plots of the pressure coefficient on the surfaces of the elements at angles of attack of 0.0, 8.13, and 14.25 deg are shown in Fig. 19. Again, excellent agreement is seen, except there is once more evidence that the computation of

References

[1]Kusunose, K., Wigton, L., and Meredith, P., "A Rapidly Converging Viscous/Inviscid Coupling Code for Multi-Element Airfoil Configurations," AIAA Paper 91-0177, Jan. 1991.

[2]Schuster, D. M., and Birckelbaw, L. D., "Numerical Computations of Viscous Flowfields About Multiple Component Airfoils," AIAA Paper 85-0167, Jan. 1985.

[3]Barth, T. J., "Numerical Aspects of Computing Viscous High Reynolds Number Flows on Unstructured Meshes," AIAA Paper 91-0721, Jan. 1991.

[4]Mavriplis, D., "Turbulent Flow Calculations Using Unstructured and Adaptive Meshes," Inst. for Computer Applications in Science and Engineering, Rept. 90-61, Hampton, VA, Sept. 1990.

[5]Benek, J. A., Buning, P. G., and Steger, J. L., "A 3-D Chimera Grid Embedding Technique," AIAA 7th Computational Fluid Dynamics Conf., AIAA Paper 85-1523-CP, Cincinnati, OH, July 1985, pp. 322–331.

[6]Valarezo, W. O., Dominik, C. J., and McGhee, R. J., "Reynolds

and Mach Number Effects on Multielement Airfoils," *Proceedings of the Fifth Symposium on Numerical and Physical Aspects of Aerodynamic Flows*, California State Univ., Long Beach, CA, Jan. 1992.

[7]Rogers, S. E., and Kwak, D., "An Upwind Differencing Scheme for the Steady-State Incompressible Navier-Stokes Equations," *Journal of Applied Numerical Mathematics*, Vol. 8, Jan. 1991, pp. 43–64.

[8]Rogers, S. E., and Kwak, D., "An Upwind Differencing Scheme for the Time Accurate Incompressible Navier-Stokes Equations," AIAA Paper 88-2583, June 1988; see also *AIAA Journal*, Vol. 28, Feb. 1990, pp. 253–262.

[9]Rogers, S. E., Kwak, D., and Kiris, C., "Numerical Solution of the Incompressible Navier-Stokes Equations for Steady-State and Time-Dependent Problems," AIAA Paper 89-0463, Jan. 1989; see also *AIAA Journal*, Vol. 29, April 1991, pp. 603–610.

[10]Chorin, A. J., "A Numerical Method for Solving Incompressible Viscous Flow Problems," *Journal of Computational Physics*, Vol. 2, Aug. 1967, pp. 12–26.

[11]Roe, P. L., "Approximate Riemann Solvers, Parameter Vectors, and Difference Schemes," *Journal of Computational Physics*, Vol. 43, Oct. 1981, pp. 357–372.

[12]Rogers, S. E., "On the Use of Implicit Line-Relaxation and Multi-Zonal Computations," AIAA 10th Computational Fluid Dynamics Conf., AIAA Paper 91-1611-CP, Honolulu, HI, June 1991, pp. 953, 954.

[13]Baldwin, B., and Barth, T., "A One-Equation Turbulence Transport Model for High Reynolds Number Wall-Bounded Flows," NASA TM 102847, Aug. 1990.

[14]Baldwin, B., and Barth, T., "A One-Equation Turbulence Transport Model for High Reynolds Number Wall-Bounded Flows," AIAA Paper 91-0610, Jan. 1991.

[15]Baldwin, B., and Lomax, H., "Thin Layer Approximation and Algebraic Model for Separated Turbulent Flows," AIAA Paper 78-257, Jan. 1978.

[16]Cordova, J. Q., and Barth, T. J., "Grid Generation for General 2-D Regions Using Hyperbolic Equations," AIAA Paper 88-0520, Jan. 1988.

[17]Coles, D., and Wadcock, A. J., "Flying-Hot-Wire Study of Flow Past an NACA 4412 Airfoil at Maximum Lift," *AIAA Journal*, Vol. 17, April 1979, pp. 321–329.

[18]Adair, D., and Horne, W. C., "Turbulent Separated Flow over and Downstream of a Two-Element Airfoil," *Experiments in Fluids*, Vol. 7, No. 8, 1989, pp. 531–541.

[19]Valarezo, W. O., Dominik, C. J., McGhee, R. J., Goodman, W. L., and Paschal, K. B., "Multi-Element Airfoil Optimization for Maximum Lift at High Reynolds Numbers," AIAA Paper 91-3332, Sept. 1991.

[20]Omar, E., Zierten, T., Hahn, M., Szpiro, E., and Mahal, A., "Two-Dimensional Wind-Tunnel Tests of a NASA Supercritical Airfoil with Various High-Lift Systems," NACA CR-2215, Sept. 1973.